

# GenCorres: Consistent Shape Matching via Coupled Implicit-Explicit Shape Generative Models

Haitao Yang<sup>1</sup> Xiangru Huang<sup>2</sup> Bo Sun<sup>1</sup> Chandrajit Bajaj<sup>1</sup> Qixing Huang<sup>1</sup>  
<sup>1</sup>The University of Texas at Austin <sup>2</sup>MIT CSAIL

## Abstract

This paper introduces *GenCorres*, a novel unsupervised joint shape matching (JSM) approach. The basic idea of *GenCorres* is to learn a parametric mesh generator to fit an unorganized deformable shape collection while constraining deformations between adjacent synthetic shapes to preserve geometric structures such as local rigidity and local conformality. *GenCorres* presents three appealing advantages over existing JSM techniques. First, *GenCorres* performs JSM among a synthetic shape collection whose size is much bigger than the input shapes and fully leverages the data-driven power of JSM. Second, *GenCorres* unifies consistent shape matching and pairwise matching (i.e., by enforcing deformation priors between adjacent synthetic shapes). Third, the generator provides a concise encoding of consistent shape correspondences. However, learning a mesh generator from an unorganized shape collection is challenging. It requires a good initial fitting to each shape and can easily get trapped by local minimums. *GenCorres* addresses this issue by learning an implicit generator from the input shapes, which provides intermediate shapes between two arbitrary shapes. We introduce a novel approach for computing correspondences between adjacent implicit surfaces and force the correspondences to preserve geometric structures and be cycle-consistent. Synthetic shapes of the implicit generator then guide initial fittings (i.e., via template-based deformation) for learning the mesh generator. Experimental results show that *GenCorres* considerably outperforms state-of-the-art JSM techniques on benchmark datasets. The synthetic shapes of *GenCorres* preserve local geometric features and yield competitive performance gains against state-of-the-art deformable shape generators.

## 1. Introduction

Shape matching is a long-standing problem with rich applications in texture transfer [76], compatible remeshing [49], shape morphing [21], deformation transfer [82], to name just a few. High-quality inter-shape correspondences are also foundations for analyzing and processing shape collections [47, 39, 38]. As the sizes and variations of geometric shape collections continue to grow, there

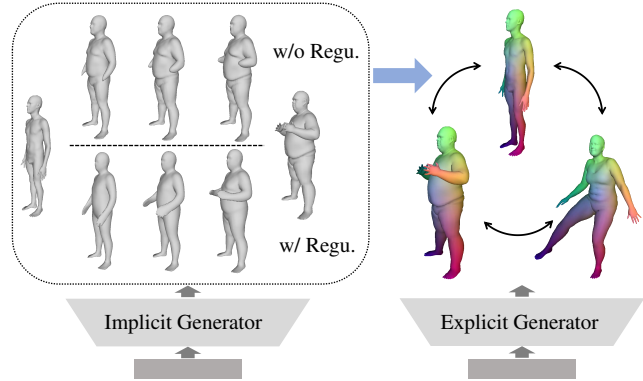


Figure 1. *GenCorres* performs consistent shape matching by learning a coupled implicit and mesh (explicit) generator from a shape collection without pre-defined correspondences. (Left) Interpolation between a pair of shape in the shape space. Constraining deformations between adjacent synthetic shapes with the regularization loss improves the shape space. (Right) The mesh generator provides consistent correspondences between pairs of shapes.

present fundamental challenges in formulating and solving the shape matching problems. Pairwise approaches work for similar shape pairs and become less effective on less similar shapes. The fundamental challenges lie in formulating suitable matching potentials (that factor out usually unknown inter-shape variations) and non-convexity in the induced non-convex optimization problems.

In contrast to pairwise matching, joint shape matching (JSM) simultaneously optimizes consistent correspondences among a shape collection [62, 41, 47, 35, 89, 39, 46, 45, 42]. These techniques bypass the difficulty of matching two less similar shapes through paths of similar shape pairs. State-of-the-art approaches typically formulate JSM as constrained low-rank recovery [35, 39, 42], where the low-rank prior serves as a regularization to prune incorrect correspondences. Despite significant advances on this topic, existing approaches present three challenges. The first is to obtain a sufficiently large dataset so that each shape has good neighboring shapes where shape matching succeeds. The second is that pairwise inputs are usually detached from joint matching. Third, encoding consistent dense correspondences is costly for large shape collections.

This paper presents *GenCorres* for solving the JSM problem. *GenCorres* takes motivations from recent advances in neural shape generators. Given a collection

of shapes with no inter-shape correspondences, GenCorres seeks to learn a mesh generator to fit the input shapes while constraining deformations between adjacent synthetic shapes to preserve geometric structures such as local rigidity and conformality (See Figure 1). Interestingly, the simple framework addresses all the challenges of JSM. GenCorres performs JSM among synthetic shapes, whose size is much larger than the number of input shapes. Second, shape matching is done among neighboring shapes through the local rigidity and local conformality potentials, bypassing the difficulty of crafting a non-linear objective function between less similar shapes. In addition, GenCorres unifies pairwise matching (i.e., through deformation priors between adjacent shapes) and consistent matching (i.e., through the generator). Furthermore, the mesh generator is analogous to the low-rank factorization in traditional JSM approaches, providing an efficient encoding of shape correspondences.

However, learning the mesh generator directly from the input shapes is challenging as it requires good initializations and optimization procedures (e.g., that minimize the earth-mover distances between synthetic shapes and training shapes [24, 1]) can easily get trapped into local minimums. GenCorres addresses this issue by learning an implicit shape generator from the input shapes. The formulation builds on a novel approach for establishing dense correspondences between adjacent implicit surfaces defined by the shape generator. These correspondences are forced to preserve local rigidity and conformality between pairs of adjacent shapes and satisfy the cycle consistency constraint among triplets of adjacent shapes. These constraints are modeled as regularization terms for learning the implicit shape generator. GenCorres then converts the learned implicit generator into an explicit mesh generator. The implicit generator offers initial consistent correspondences by guiding template-based registration. It also provides shape regularizations for learning the mesh generator.

We have evaluated GenCorres on various deformable shape collections, including humans and animals. Experimental results show that GenCorres outperform state-of-the-art JSM approaches and implicit shape generators, making GenCorres a universal framework for computing JSM and learning deformable implicit shape generators. An ablation study justifies the importance of different components of GenCorres. Codes will be available at <https://github.com/yanghr/GenCorres>.

## 2. Related Works

We discuss the relevant works under five topics, namely, pairwise shape matching, joint shape matching, generative model based matching, matching under implicit representations, and implicit neural representations.

**Pairwise shape matching.** Pairwise shape matching has been studied extensively in the literature [73, 86, 48, 63, 2, 59, 60]. Most of them formulate matching potentials and develop techniques to solve the induced optimization problems (c.f. [86]). A recent line of works establishes a learning framework under the functional map representa-

tion [55, 32, 16, 16, 77]. However, existing techniques still do not work well for less similar shape pairs, where it is difficult to learn suitable matching objective functions.

NeuroMorph [21] is another learning framework that combines a correspondence module and a shape interpolation module. The network is trainable in an unsupervised manner by enforcing the consistency between these two modules and an alignment loss. Several other works [19, 18] also studied how to optimize interpolation paths to establish correspondences. While GenCorres is relevant to these approaches, GenCorres is a data-driven approach that uses an implicit generator with learned feature representations from all input shapes to drive pairwise matching. In contrast, these approaches are not data-driven.

**Joint shape matching.** The underlying principle of joint shape matching (JSM) techniques [62, 41, 47, 35, 89, 39, 11, 46, 45, 42] is cycle-consistency, which states that composition maps along cycles should approximate the identity maps [62, 35]. State-of-the-art JSM techniques use the equivalence between the cycle-consistency constraint and the low-rank property of the data matrix which encodes pairwise maps in blocks (c.f. [35]). This leads to constrained low-rank matrix recovery approaches [35, 89, 11, 44, 7, 46], which possess strong theoretical guarantees.

GenCorres advances JSM in multiple ways. First, JSM’s performance improves when the input collection size increases, as each shape can have more neighboring shapes where the shape matching problem is easier to solve [62, 41, 47, 35]. The advantage of GenCorres is that it performs synchronization among the large collection of synthetic shapes and fully uses the data-driven behavior of JSM.

Second, in prior works joint matching and pairwise matching are typically decoupled. The major difficulty is that the representations and optimization algorithms used in many pairwise matching techniques are not friendly to JSM. CZO [42] is an exception, yet it still requires good initializations, e.g., [48]. In contrast, GenCorres unifies pairwise matching and joint matching under a simple formulation. Cycle-consistency is automatically enforced through the generator, which is analogous to the low-rank factorization in standard JSM formulations [35, 64, 89, 11, 44, 7]. Moreover, JSM performs pairwise matching among neighboring shapes through simple geometric regularizations.

Finally, JSM still requires storing consistent matches across the input shape collection [41, 47, 39]. This approach becomes impractical for large shape collections. GenCorres addresses this issue by using a shape generator to effectively compresses consistent correspondences.

**Generative model based correspondences.** Generative models under explicit representations provide inter-shape correspondences. This property makes them appealing for practical applications. However, existing methods are sub-optimal for high-fidelity correspondence computation. Most mesh-based generators [83, 87, 53, 85, 69] require consistent dense correspondences as input, and the trained generators are sensitive to correspondence quality. In contrast to mesh-based generators, point-based generators [24, 1, 91, 50, 52] do not require inter-shape correspondences.

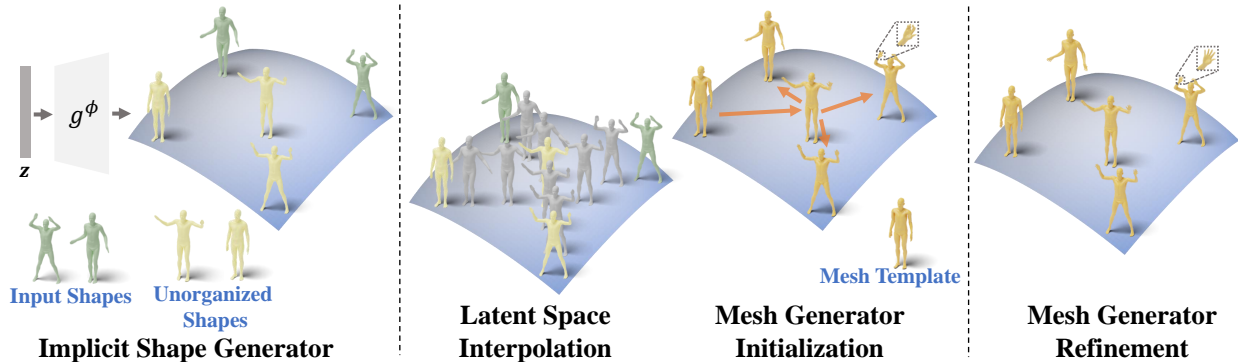


Figure 2. GenCorres has three stages. The first stage learns an implicit shape generator from the input shapes and an unorganized shape collection. The training loss regularizes the induced correspondences between adjacent implicit shapes of the generator. The second stage uses the implicit generator to initialize a mesh generator through latent space interpolation and template matching. The third stage then refines the mesh generator with ACAP energy.

The downside is that a point cloud is permutation-invariant. Therefore, the point indices in a point cloud do not always reflect meaningful correspondences. GenCorres addresses these limitations by performing shape matching under implicit representations using shape-preserving potentials.

Several works studied shape matching in embedding spaces. [90, 14] learn encoding networks so that corresponding points are aligned in embedding spaces. [56] introduced an unsupervised approach that combines a decoder that maps each input shape into a latent space and an encoder that maps it back to the ambient space. [13] proposed a spherical space to encode inter-shape correspondences. The advantages of GenCorres are two-fold. First, GenCorres utilizes synthetic shapes to propagate correspondences. Second, GenCorres employs a cycle-consistent constraint to further enhance the implicit generator.

3D-CODED [29] adopts an auto-encoder to deform a template shape for shape matching. Training can be done in an unsupervised manner by combining the Chamber distance for shape alignment and regularizations on Laplacian operators and edge lengths. As the regularizations of 3D-CODED are designed for isometric deformations and training is driven by the Chamfer distance, they are mostly applicable to small inter-shape variations. In contrast, GenCorres performs shape matching among neighboring synthetic shapes and enforces the cycle-consistency constraint among propagated correspondences between less similar shapes. It applies to shape collections under large deformations.

**Matching under implicit surfaces.** A fundamental problem for neural implicit shape representation is how to define inter-shape correspondences when the implicit surface undergoes infinitesimal changes. The technical challenge is that there is only one constraint along the normal direction at each surface point, c.f., [81]. GenCorres solves a constrained optimization problem to obtain inter-shape correspondences. A relevant formulation has been studied in [84]. However, GenCorres innovates in using an objective function that preserves local shapes. Under the implicit representation, a popular way to regularize local rigidity is to enforce the Killing vector field constraint [8, 79, 84, 78], which is correspondence-free. In contrast, GenCorres aims

at computing correspondences between implicit surfaces.

**Implicit neural representations** Thanks to flexibilities in modeling shape details and topological variabilities, neural implicit representations have received great interests on modeling 3D shapes, including man-made objects [65, 61, 12, 15] and deformable objects [74, 75, 3, 67]. Unlike developing novel implicit network architectures, GenCorres focuses on regularization losses that enforce geometric priors for deformable objects.

Developing regularization losses for training implicit neural networks has also been studied recently [27, 6]. GenCorres is most relevant to [6], which uses an as-killing-as possible regularization loss to preserve global rigidity. In contrast, GenCorres focuses on preserving local rigidity/conformality, which better aligns with the underlying geometric variations of deformable objects.

GenCorres is also relevant to ARAPReg [36]. However, defining a suitable loss under the implicit representation has to address the fundamental challenge of defining inter-shape correspondences. GenCorres also enforces the cycle-consistency constraint among induced shape correspondences to enhance the implicit generator.

### 3. Problem Statement and Approach Overview

**Problem statement.** The input to GenCorres is a shape collection  $\mathcal{S} = \{S_1, \dots, S_n\} \subset \bar{\mathcal{S}}$ , where  $\bar{\mathcal{S}}$  is the underlying shape space. Each shape  $S_i$  can be a raw mesh or a raw point cloud. We do not assume that they have pre-defined correspondences.

GenCorres seeks to learn a mesh generator  $g^\theta : \mathcal{Z} \rightarrow \bar{\mathcal{S}}$  where  $\mathcal{Z} := \mathbb{R}^d$  denotes the latent space. Our goal is to align each input shape  $S_i$  with the corresponding synthetic shape  $g^\theta(z_i)$  where  $z_i \in \mathbb{R}^d$  is the latent code of  $S_i$ . The resulting mesh generator provides consistent correspondences since all the generated meshes share the same topology.

**Approach overview.** As illustrated in Fig. 2, GenCorres proceeds in three stages. The first two stages provide initializations for the third stage, which learns the mesh generator. Specifically, the first stage adopts variational auto-encoder (VAE) to learn an implicit generator  $g^\phi : \mathbb{R}^3 \times \mathcal{Z} \rightarrow \mathbb{R}$

and an encoder  $h^\psi$  from the input shapes, bypassing the difficulty of training a mesh generator without pre-defined correspondences.

$$\min_{\phi, \psi \{z_i\}} l_{\text{VAE}}(g^\phi, h^\psi) + \lambda_{\text{geo}} r_{\text{geo}}(g^\phi) + \lambda_{\text{cyc}} r_{\text{cyc}}(g^\phi) \quad (1)$$

where  $l_{\text{VAE}}$  is a VAE loss on the training shapes.  $r_{\text{geo}}(g^\phi)$  and  $r_{\text{cyc}}(g^\phi)$ , which are key contributions of this paper, build on novel induced correspondences between adjacent implicit shapes defined by  $g^\phi$ . Specifically,  $r_{\text{geo}}(g^\phi)$  enforces that the induced correspondences preserve local geometric structures.  $r_{\text{cyc}}(g^\phi)$  enforces that the induced correspondences are cycle-consistent among triplets of adjacent shapes. In other words,  $r_{\text{geo}}(g^\phi)$  and  $r_{\text{cyc}}(g^\phi)$  perform pairwise matching and consistent matching, respectively.

The second stage of GenCorres fits a template mesh to all input shapes along paths of interpolated shapes provided by the implicit shape generator. The resulting correspondences are used to learn an initial mesh generator  $g^\theta$ .

The third stage of GenCorres refines the mesh generator by solving another optimization problem:

$$\min_{\theta} d_{\text{exp}}(g^\theta(z), \bar{\mathcal{S}}) + \lambda_d r_d(g^\theta(z)) \quad (2)$$

where  $d_{\text{exp}}(g^\theta(z), \bar{\mathcal{S}})$  aligns the explicit generator with the input shape collection;  $r_d(g^\theta)$  enforces ACAP deformation prior among adjacent shapes.

## 4. Stage I: Implicit Shape Generator

This section introduces how to learn the implicit shape generator  $g^\phi$ . We begin with a novel approach for computing dense correspondences between adjacent synthetic implicit surfaces in Section 4.1. Based on the induced correspondences, we introduce two regularization terms  $r_{\text{geo}}(g^\phi)$  and  $r_{\text{cyc}}(g^\phi)$  in Section 4.2 and Section 4.3, respectively. Finally, Section 4.4 elaborate on the implementation details.

### 4.1. Induced Shape Correspondences

Our goal is to compute dense correspondences between the implicit surface  $g^\phi(\mathbf{x}, \mathbf{z}) = 0$  and an adjacent implicit surface  $g^\phi(\mathbf{x}, \mathbf{z} + \epsilon \mathbf{v}) = 0$ , where  $\mathbf{v} \in \mathbb{R}^d$  is a direction in the unit ball  $\mathcal{B}^d$  and  $\epsilon$  is an infinitesimal value. To this end, we discretize  $g^\phi(\mathbf{x}, \mathbf{z}) = 0$  using a mesh with  $n$  vertices  $\mathbf{g}^\phi(\mathbf{z}) \in \mathbb{R}^{3n}$ , e.g., via Marching cube [57], and compute the corresponding vertices  $\mathbf{g}^\phi(\mathbf{z} + \epsilon \mathbf{v}) := \mathbf{g}^\phi(\mathbf{z}) + \epsilon \mathbf{d}^v(\mathbf{z}) \in \mathbb{R}^{3n}$  on  $g^\phi(\mathbf{x}, \mathbf{z} + \epsilon \mathbf{v}) = 0$ . As discussed in [81, 84], the implicit representation offers one constraint on each  $\mathbf{d}_i^v(\mathbf{z})$  along the normal direction:

$$\frac{\partial g^\phi}{\partial \mathbf{x}}(\mathbf{g}_i^\phi(\mathbf{z}), \mathbf{z})^T \mathbf{d}_i^v(\mathbf{z}) + \frac{\partial g}{\partial \mathbf{z}}(\mathbf{g}_i^\phi(\mathbf{z}), \mathbf{z})^T \mathbf{v} = 0. \quad (3)$$

As (3) only provides one constraint on  $\mathbf{d}_i^v(\mathbf{z})$ , we determine  $\mathbf{d}^v(\mathbf{z})$  by enforcing that the displacements of the 1-ring patch at each vertex  $\mathbf{g}_i^\phi(\mathbf{z})$  are as-rigid-as possible (ARAP) [40, 36] and as-conformal-as possible

(ACAP) [92]. Specifically, let  $I_3 + \mathbf{c}_i \times$  be the latent linearized rotation at  $\mathbf{g}_i^\phi(\mathbf{z})$ . We define the ARAP potential on  $\mathbf{d}^v(\mathbf{z})$  as

$$\sum_{i=1}^n \min_{\mathbf{c}_i} \sum_{j \in \mathcal{N}_i} \|\mathbf{c}_i \times (\mathbf{g}_i^\phi(\mathbf{z}) - \mathbf{g}_j^\phi(\mathbf{z})) - (\mathbf{d}_i^v(\mathbf{z}) - \mathbf{d}_j^v(\mathbf{z}))\|^2 \\ = \mathbf{d}^v(\mathbf{z})^T \bar{L}^{\text{arap}}(\mathbf{g}^\phi(\mathbf{z})) \mathbf{d}^v(\mathbf{z}) \quad (4)$$

where the expression of  $\bar{L}^{\text{arap}}(\mathbf{g}^\phi(\mathbf{z}))$  is in the supp. material.

Similarly, we can parameterize the latent linearized similarity transformation at  $\mathbf{g}_i^\phi(\mathbf{z})$  as  $(1 + s_i)I_3 + \mathbf{c}_i \times$  and define the ACAP potential as

$$\sum_{i=1}^n \min_{s_i, \mathbf{c}_i} \sum_{j \in \mathcal{N}_i} \|(s_i I_3 + \mathbf{c}_i \times)(\mathbf{g}_i^\phi(\mathbf{z}) - \mathbf{g}_j^\phi(\mathbf{z})) - (\mathbf{d}_i^v(\mathbf{z}) - \mathbf{d}_j^v(\mathbf{z}))\|^2 \\ = \mathbf{d}^v(\mathbf{z})^T \bar{L}^{\text{acap}}(\mathbf{g}^\phi(\mathbf{z})) \mathbf{d}^v(\mathbf{z}) \quad (5)$$

where the expression of  $\bar{L}^{\text{acap}}(\mathbf{g}^\phi(\mathbf{z}))$  is in the supp. material.

Denote  $\bar{L}^\phi(\mathbf{z}) = \alpha \bar{L}^{\text{arap}}(\mathbf{g}^\phi(\mathbf{z})) + \bar{L}^{\text{acap}}(\mathbf{g}^\phi(\mathbf{z}))$  where  $\alpha$  is a tradeoff parameter ( $\alpha = 10$  in our experiments). We compute  $\mathbf{d}^v(\mathbf{z})$  via linearly constrained quadratic programming:

$$\mathbf{d}^v(\mathbf{z}) := \lim_{\mu \rightarrow 0} \underset{\mathbf{d}}{\text{argmin}} \quad \mathbf{d}^T \bar{L}^\phi(\mathbf{z}) \mathbf{d} + \mu \|\mathbf{d}\|^2 \\ \text{s.t.} \quad C^\phi(\mathbf{z}) \mathbf{d} = -F^\phi(\mathbf{z}) \mathbf{v} \quad (6)$$

where  $C^\phi(\mathbf{z}) \mathbf{d} = -F^\phi(\mathbf{z}) \mathbf{v}$  is the matrix representation of (3),  $C^\phi(\mathbf{z}) \in \mathbb{R}^{n \times 3n}$  is a block diagonal sparse matrix,  $F^\phi(\mathbf{z}) \in \mathbb{R}^{n \times d}$ ,  $\mu$  is used to avoid degenerate cases, e.g., a rotating sphere. It is easy to check that

$$\mathbf{d}^v(\mathbf{z}) = -G^\phi(\mathbf{z}) \mathbf{v}, \quad (7) \\ G^\phi(\mathbf{z}) := \bar{L}^\phi(\mathbf{z})^+ C^\phi(\mathbf{z})^T (C^\phi(\mathbf{z}) \bar{L}^\phi(\mathbf{z})^+ C^\phi(\mathbf{z})^T)^+ F^\phi(\mathbf{z})$$

where  $A^+$  denotes the MP-pseudo inverse of  $A$ .

### 4.2. Geometric Deformation Regularization Loss

We proceed to introduce the first regularization loss  $r_{\text{geo}}(g^\phi)$ . The idea is to penalize local rigidity and local conformality distortions of the induced correspondences from  $g^\phi(\mathbf{x}, \mathbf{z}) = 0$  to  $g^\phi(\mathbf{x}, \mathbf{z} + \epsilon \mathbf{v}) = 0$ :

$$r_{\text{geo}}(g^\phi, \mathbf{z}, \mathbf{v}) := \mathbf{d}^v(\mathbf{z})^T \bar{L}^\phi(\mathbf{z}) \mathbf{d}^v(\mathbf{z}) = \mathbf{v}^T E^\phi(\mathbf{z}) \mathbf{v} \quad (8) \\ E^\phi(\mathbf{z}) := F^\phi(\mathbf{z})^T (C^\phi(\mathbf{z}) \bar{L}^\phi(\mathbf{z})^+ C^\phi(\mathbf{z})^T)^+ F^\phi(\mathbf{z})$$

Integrating  $\mathbf{v}$  over the unit ball  $\mathcal{B}^d$  in  $\mathbb{R}^d$  [37], we arrive at

$$r_{\text{geo}}(g^\phi) = E_{\mathbf{z} \sim \mathcal{N}_d} \int_{\mathbf{v} \in \mathcal{B}_d} \mathbf{v}^T E^\phi(\mathbf{z}) \mathbf{v} d\mathbf{v} \\ = E_{\mathbf{z} \sim \mathcal{N}_d} \frac{\text{Vol}(\mathcal{B}_d)}{d} \text{Tr}(E^\phi(\mathbf{z})) \quad (9)$$



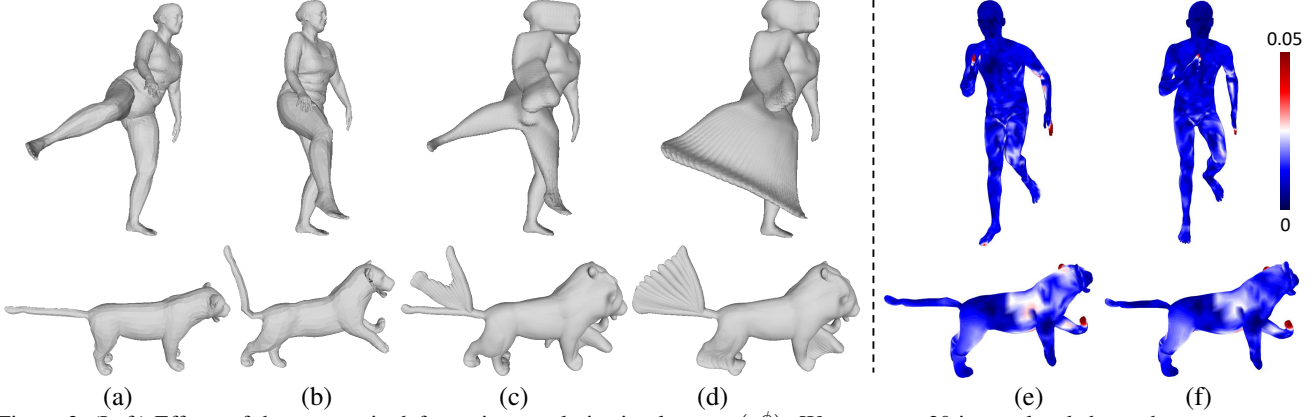


Figure 3. (Left) Effects of the geometric deformation regularization loss  $r_{\text{geo}}(g^\phi)$ . We compute 30 interpolated shapes between a source shape (a) and a target shape (b) via linear interpolation between their latent codes. All the interpolated shapes are visualized in the same coordinate system. (c) Interpolation results without  $r_{\text{geo}}(g^\phi)$ . (d) With  $r_{\text{geo}}(g^\phi)$ . (Right) Effects of the cycle-consistency regularization loss  $r_{\text{cyc}}(g^\phi)$ . We color-code errors of propagated correspondences through a path of intermediate shapes between each source-target shape pair. The error is visualized on the target mesh. (e) Without  $r_{\text{cyc}}(g^\phi)$ . (f) With  $r_{\text{cyc}}(g^\phi)$ .

Figure 3 (Left) shows that  $r_{\text{geo}}$  can improve the quality of the implicit shape generator. The interpolated shapes are smoother and more shape-preserving, meaning the learned shape space is better.

### 4.3. Cycle-Consistency Regularization Loss

The induced correspondences defined in (7) enable us to compute correspondences between two shapes by composing induced correspondences along a path of intermediate shapes. An additional regularization we can enforce is that the induced correspondences are cycle-consistent. To this end, we constrain 3-cycle consistency [35] among three neighboring synthetic shapes  $g(\mathbf{x}, \mathbf{z}) = 0$ ,  $g(\mathbf{x}, \mathbf{z} + \epsilon \mathbf{v}) = 0$ , and  $g(\mathbf{x}, \mathbf{z} + \epsilon \mathbf{v}') = 0$ , where  $\mathbf{v}$  and  $\mathbf{v}'$  are two different displacement vectors. Formally speaking, we model 3-cycle distortion as

$$\begin{aligned} \mathbf{r}^{v, v'}(\mathbf{z}) &:= \mathbf{d}^v(\mathbf{z}) + \mathbf{d}^{v' - v}(\mathbf{z} + \epsilon \mathbf{v}) - \mathbf{d}^{v'}(\mathbf{z}) \\ &\approx -\epsilon (\mathbf{v}^T \frac{\partial G^\phi(\mathbf{z})}{\partial \mathbf{z}}) (\mathbf{v} - \mathbf{v}'). \end{aligned} \quad (10)$$

Based on (10), we define the cycle-consistency regularization term as

$$r_{\text{cyc}}(g^\phi) = E_{\mathbf{z} \sim \mathcal{N}_d} \int_{\mathbf{v} \in \mathcal{B}^d} \left\| \frac{\partial G^\phi(\mathbf{z})}{\partial \mathbf{z}} \right\|_{\mathcal{F}}^2 \cdot d\mathbf{v} \quad (11)$$

where  $\|\cdot\|_{\mathcal{F}}$  is the tensor Frobenius norm. We use finite-difference to compute  $r_{\text{cyc}}(g^\phi)$ . Specifically, we compute

$$\left\| \frac{G^\phi(\mathbf{z} + \epsilon_{\text{cyc}} \mathbf{e}_i) - G^\phi(\mathbf{z})}{\epsilon_{\text{cyc}}} \right\|_{\mathcal{F}}^2$$

as an approximation of  $r_{\text{cyc}}(g^\phi)$ , where  $\epsilon_{\text{cyc}} = 1e^{-3}$  and  $\mathbf{e}_i$  is a random standard basis in  $\mathbb{R}^d$ .

As illustrated in Figure 3 (Right), the cycle-consistency regularization loss (11) can enhance the quality of inter-shape correspondences through correspondence computation as well as the implicit generator.

### 4.4. Implementation Details

We use the VAE network proposed in SALD [5], where the encoder  $h^\psi$  is a modified PointNet [68] and the decoder  $g^\phi$  is an 8-layer MLP. The data loss  $l_{\text{VAE}}$  is the VAE loss of SALD. We set  $\lambda_{\text{geo}} = 1e^{-3}$ ,  $\lambda_{\text{cyc}} = 1e^{-4}$ , and  $\epsilon = 1e^{-3}$ . We use autograd in PyTorch [66] to compute  $F^\phi(\mathbf{z})$  and  $C^\phi(\mathbf{z})$ . For other derivative computation, we use fine-difference for approximation. More details are deferred to the supp. material.

### 5. Stage II: Mesh Generator Initialization

The second stage initializes the mesh generator  $g^\theta$  using the implicit shape generator  $g^\phi$  obtained in stage I. Gen-Corres uses the same mesh generator as ARAPReg [36], which maps the latent code  $\mathbf{z}$  to displacement vectors associated with vertices of a template mesh  $\mathcal{M}$ . We use the learned encoder  $h^\psi$  to find the latent code  $\mathbf{z}_{\text{temp}}$  of  $\mathcal{M}$ . Let  $\mathbf{z}_i = h^\psi(S_i)$  be the latent code of the input shape  $S_i$ . We generate  $m$  intermediate shapes  $g^\phi(\mathbf{z}_i^j)$ ,  $1 \leq j \leq m$  ( $m = 10$  in our experiments) by linearly interpolating  $\mathbf{z}_{\text{temp}}$  and  $\mathbf{z}_i$ :  $\mathbf{z}_i^j = \mathbf{z}_{\text{temp}} + j \frac{\mathbf{z}_i - \mathbf{z}_{\text{temp}}}{m+1}$ . We then apply non-rigid registration to align the template mesh  $\mathcal{M}$  with each intermediate shape  $g^\phi(\mathbf{z}_i^j)$  in order, i.e., the alignment of one intermediate shape provides the initialization for aligning the next intermediate shape. Non-rigid alignment adapts an ARAP deformation energy, and the details are deferred to the supp. material.

After propagating the correspondences along the interpolation path in the shape space, we obtain the deformed template  $\mathbf{g}_i^{\text{init}}$  for each input shape  $S_i$ . We then initialize the mesh generator  $g^\theta$  using the standard regression loss:

$$\theta^{\text{init}} = \underset{\theta}{\operatorname{argmin}} \sum_{i=1}^n \|\mathbf{g}_i^{\text{init}} - \mathbf{g}^\theta(\mathbf{z}_i)\|^2. \quad (12)$$

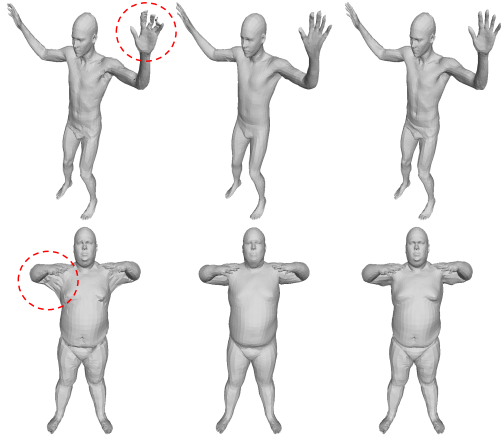


Figure 4. The mesh generator improves the inter-shape correspondences by learning better shape generation. From left to right: the deformed template from stage II, the shape generated by the mesh generator and the input raw mesh.

### 6. Stage III: Mesh Generator Refinement

The third stage refine the mesh generator  $g^\theta(z)$  by solving (2). To this end, we define the distance between the mesh generator and the input shape collection as

$$d_{\text{exp}}(g^\theta(z), \bar{\mathcal{S}}) := \frac{1}{n} \sum_{i=1}^n l_{\text{CD}}(g^\theta(z_i), \mathcal{S}_i). \quad (13)$$

where  $g^\theta(z_i)$  is the  $i$ -th generated mesh,  $l_{\text{CD}}$  is the Chamfer loss. Since the mesh generator has a good initialization, the loss is easy to optimize. As (13) only constrains that vertices of the mesh generator lie on the surface, merely minimizing it does not prevent drifting. To address this issue, we define the regularization term  $r_d(g^\theta)$  to enforce that the deformations between meshes with similar latent codes preserve geometric structures. As the implicit generator already constrains the global shape of the mesh generator, we enforce the deformations to be ACAP, which allows the mesh generator to capture large non-rigid deformations. Based on (5), we define

$$r_d(g^\theta) = \mathbb{E}_{z \sim \mathcal{N}_d} \int_{v \in \mathbb{B}^d} v^T \frac{\partial g^\theta(z)}{\partial z}^T L^{\text{acap}}(g^\theta(z)) \frac{\partial g^\theta(z)}{\partial z} v dv. \quad (14)$$

We then substitute (13) and (14) into (2) to refine the mesh generator. Note that in this refinement stage, the mesh generator is optimized to fit all input shapes together while enforcing the ACAP deformation prior among adjacent surfaces. In contrast, the initialization stage optimizes an ACAP deformation between the template mesh and each input shape in isolation.

As shown in Figure 4, the mesh generator can improve the shape quality from the implicit generator. Since the mesh generator directly provides consistent correspondences, higher shape generation quality implies better inter-shape correspondences.

## 7. Experimental Evaluation

This section presents an experimental evaluation of GenCorres. We begin with the experimental setup in Section 7.1. Section 7.2 compares GenCorres with state-of-the-art unsupervised shape matching approaches. Section 7.3 then compares GenCorres against state-of-the-art learning-based pair-wise shape matching approaches. We proceed to evaluate the shape generator quality of GenCorres in Section 7.4. Finally, Section 7.5 presents an ablation study.

### 7.1. Experimental Setup

**Datasets.** We evaluate GenCorres on two categories of deformable shape collections, i.e., Human and Animal. The Human category has two datasets, DFAUST and FAUST. We use the registered SMPL model from the original DFAUST dataset. Since there is low variety between the adjacent shapes, we subsample 2000 meshes from the original dataset. For FAUST, we use the re-meshed version [71], which contains 100 meshes with different topologies. Animal category has one dataset of 383 shapes [36], which is generated from SMAL [94]. We defer the details of dataset processing to the supp. material.

**Evaluation protocols.** For correspondence evaluation, we report the median the mean geodesic errors of the predicted correspondences from between involved shape pairs detailed in Section 7.2 and Section 7.3.

We evaluate the shape generation quality via reconstruction errors of testing shapes. We define the reconstructing error as the Chamfer distance between the reconstructed mesh and the raw testing shape.

### 7.2. Evaluation on Unsupervised Shape Matching

Table 1 reports statistics of GenCorres for JSM on DFAUST and SMAL. For baseline comparison, we choose consistent zoom out (CZO) [43] and multiple isometric matching (MIM) [25], which are two state-of-the-art JSM approaches. Overall, GenCorres outperforms state-of-the-art JSM baselines by large margins. Specifically, GenCorres reduces the mean/median errors by 47.8%/54.3% and 14.3%/58.0% on DFAUST and SMAL, respectively. The performance gains come from two aspects. First, enforcing ARAP and ACAP deformations in the shape space locally is superior to applying sophisticated deformation models between pairs of shapes directly. Second, GenCorres performs map synchronization on synthetic shapes of the generator whose size is much larger than the input shape collection used by JSM baselines.

The correspondences of the explicit generator (GenCorres) is superior to propagated correspondences of the implicit generator (GenCorres-Imp), i.e., 50.4%/37.6% and 17.8%/11.4% of error reductions on DFAUST and SMAL, respectively. Such improvements are expected as the cycle-consistency constraint is only enforced locally, and propagated correspondences between shapes that undergo large deformations may drift.

GenCorres also significantly outperforms NeuroMorph [21], a state-of-the-art pairwise shape matching

	DFAUST		SMAL	
	mean	median	mean	median
CZO [43]	3.71	3.68	1.19	1.12
MIM [25]	3.42	3.40	1.30	1.29
NeuroMorph [21]	2.49	2.47	1.59	1.43
GenCorres	<b>1.30</b>	<b>1.13</b>	<b>1.02</b>	<b>0.47</b>
GenCorres-Imp	2.62	1.81	1.24	0.53
GenCorres-NoCycle	1.41	1.22	1.11	0.51
GenCorres-NoReg	7.65	7.34	6.28	5.09
GenCorres-NoACAP	1.62	1.42	1.07	0.49

Table 1. Evaluations of inter-shape correspondences on DFAUST and SMAL dataset. For each method, we report of mean and median geodesic error (in cm) of correspondences from the template model to other models. Qualitative results are in the supp. material

technique (See Table 1). As shown in Figure 5, GenCorres results in significant improvements around areas that have complex deformations.

### 7.3. Evaluation on Learning Pairwise Matching

Many recent state-of-the-art shape matching methods are learning based. Most of them are evaluated on FAUST [9] with 80/20 training/testing split. As GenCorres is a data-driven approach, applying it directly on 80 shapes of FAUST does not offer satisfactory results (learning a deformable shape generator from few training shapes is very difficult). To show the advantage of GenCorres against these approaches, we augment the training data of FAUST by the DFAUST dataset, resulting in 1080 shapes. We then apply GenCorres to learn a shape generator  $g^\theta$ . The inter-shape correspondences between two testing shapes are given by the correspondences induced from the template model.

For baseline comparisons, we consider state-of-the-art unsupervised deep learning (DL) approaches such as NeuroMorph [21], DeepShells [23], SurFMNet [72], Unsup. FMnet [33], and AttentiveFmaps [51]. To fully evaluate GenCorres, we also compare against supervised DL approaches 3D-CODED [31], FMnet [54], and GeoFMNet [17]. To make fair comparison, we also retrain the state-of-the-art baseline approach NeuroMorph using the augmented training dataset, dubbed NeuroMorph-L. For each baseline, we report correspondence errors of pairwise matching. For simplicity, we apply nonrigid registration as a post-processing step. More advanced post-processing techniques can also be used.

As shown in Table 2, without post processing, GenCorres outputs NeuroMorph, the top-performing unsupervised baseline approach. After post-processing, GenCorres is competitive against all baseline approaches. This behavior again shows the advantages of learning shape generators by enforcing ARAP and ARCP deformation models locally to address large inter-shape deformations over using deep neural networks to encode large inter-shape deformations that are trained in unsupervised manners. Of course, GenCorres assumes a sufficient large training set.

		error	p.p.	error w/o p.p.
Axiom.	BCICP [71]	6.4	–	–
	ZoomOut [60]	6.1	–	–
	Smooth Shells [20]	2.5	–	–
JSM	CZO [43]	2.2	–	–
	MIM [25]	2.3	–	–
Sup.	3D-CODED [30]	2.5	–	–
	FMNet [54]	5.9	PMF	11
	GeoFMnet [17]	<b>1.5</b>	ZO	2.7
Unsup.	SurFMNet [72]	7.4	ICP	15
	Unsup. FMnet [33]	5.7	PMF	10
	AttentiveFmaps [51]	1.9	–	–
	DeepShells [23]	1.7	–	–
	NeuroMorph [21]	<b>1.5</b>	SL	2.3
	NeuroMorph-L [21]	2.1	Nonrigid-ICP	3.6
GenCorres		1.6	Nonrigid-ICP	<b>2.0</b>

Table 2. Evaluations of inter-shape correspondence mean errors (in cm) on FAUST-20 dataset. Baseline approaches are described in Section 7.3. Both GenCorres and NeuroMorph-L use simple nonrigid-ICP as post-processing. Other alternatives include PMF [88], ZO [43], ICP [63], SL [20].

		DFAUST		SMAL	
		mean	median	mean	median
Point	LGF [10]	4.62	2.30	9.13	8.15
	DPM [58]	3.80	2.00	8.07	7.44
Implicit	DeepSDF [65]	2.03	1.98	7.84	7.59
	SALD [5]	1.88	1.79	7.66	7.32
GenCorres		1.83	1.75	6.85	6.81

Table 3. Evaluations of shape generator quality. For each method, we report the mean and median reconstruction errors ( $\times 10^{-2}m$ ) of the testing shapes. Baseline approaches are described in Section 7.4.

GenCorres exhibits competitive against supervised DL baselines. Without post processing, GenCorres outperforms both GeoFMNet and FMNet. with post-processing, GenCorres is competitive against GeoFMNet, the top-performing supervised baseline. One explanation of is that the size of the training data is large and it provides a nice coverage of the testing shapes. Therefore, the generators from the training shapes generalizes to testing shapes.

### 7.4. Evaluation on Shape Generation Quality

We compare with the state-of-the-art shape generation approaches that do not rely on pre-defined ground-truth correspondences. Those include implicit shape generators DeepSDF, point-based generators, such as LGF [10] and DPM [58]. For Human category, we train the shape generator from 1000 shapes and evaluate them on the remaining 1000 shapes. For the Animal category, we use 289 shapes for training and 94 shapes for testing .

Table 3 provides quantitative comparisons between GenCorres and baseline shape generators. Due to space limit,

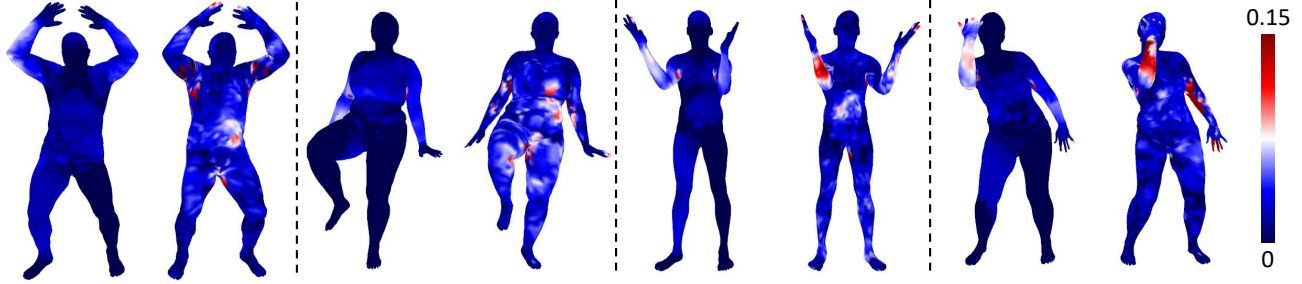


Figure 5. Visualization of correspondence errors of GenCorres and unsupervised baseline approach NeuroMorph[22]. In each group of shapes, the left is our result, the right is from NeuroMorph. We color code the correspondence errors on the target shape.

we defer the qualitative comparisons to the supplemental material. Overall, GenCorres outperforms state-of-the-art deformable shape generators both quantitatively and qualitatively. More comparisons are in the appendix.

GenCorres is superior to state-of-the-art implicit deformable shape generators in terms of both reconstruction errors and plausibility of synthetic shapes. Quantitatively, the reductions in mean/median reconstruction errors range from 2.7%-10.6%, 2.3%-7.0% on DFAUST and SMAL, respectively.

Without pre-defined correspondences, GenCorres considerably outperforms state-of-the-art point-based shape generators, including LGF, and DPM. The reductions in mean/median reconstruction errors are 51.9%/12.0% and 15.2%/8.5% on DFAUST and SMAL, respectively. The performance gains come from the implicit shape representation and geometric regularization losses employed by GenCorres.

### 7.5. Ablation Study

This section presents an ablation study on different components of GenCorres. The importance of the explicit generator is already discussed in Section 7.2. As the main purpose of GenCorres is inter-shape correspondences, we focus on how the correspondence quality changes when varying different components of GenCorres (See Table 1).

**Without the cycle-consistency term.** Figure 3 (Right) shows that the cycle-consistency term can improve the drifting issue of propagated correspondences considerably. Dropping this term hurts the quality of the implicit generator. This issue cannot be recovered when converting the implicit generator into the mesh generator. Quantitatively, the correspondence errors increase by 8.4%/7.9% and 8.8%/8.5% in mean/median on DFAUST and SMAL.

**Without the geometric regularization term** The performance of GenCorres drops considerably when removing the geometric regularization term. The mean/median geodesic errors increase by 488%/549% and 515%/982% on DFAUST and SMAL. This shows that even the cycle-consistency constraint is enforced on correspondences computed from optimizing ARAP and ACAP losses, constraining that these correspondences minimize ARAP and ACAP losses is critical for the quality of the resulting generators.

**ACAP versus ARAP** Another variant of GenCorres is to drop the ACAP regularization when learning the implicit

generator and replace the ACAP regularization with the ARAP regularization when learning the explicit generator. As shown in Table 1, the performance of GenCorres slightly decreases when merely using ARAP. In particular, on DFAUST that exhibit large inter-shape deformations, i.e., thin versus fat and low versus tall, the performance drops are considerable. Such performance gaps show that the ACAP regularization loss is important for modeling large non-isometric inter-shape deformations.

## 8. Conclusions, Limitations, and Future Work

This paper shows that learning shape generators from a collection of shapes leads to consistent inter-shape correspondences that considerably outperform state-of-the-art JSM approaches. The key novelties of GenCorres are two regularization losses that enforce geometric structures are preserved and induced correspondences are cycle-consistent. We present extensive experimental results to justify the effectiveness of these two regularization terms. Besides high-quality inter-shape correspondences, GenCorres also outperforms state-of-the-art deformable shape generators trained from unorganized shape collections.

One limitation of GenCorres is that it requires a reasonably large training dataset to train the shape generator and does not work with few training shapes. In this latter regime, learning pairwise matching has the advantage over GenCorres. This issue may be partially addressed by using a more advanced implicit generator for deformable shapes, which is an area for future research.

There are ample future directions. So far, the regularization terms are based on discretizing implicit surfaces into meshes. An interesting question is how to define them without mesh discretization. Another direction is to explore regularization terms for man-made shapes, e.g., to enhance topological generalization and promote physical stability.

**Acknowledgement.** We would like to acknowledge NSF IIS-2047677, HDR-1934932, and CCF-2019844.

## References

- [1] Panos Achlioptas, Olga Diamanti, Ioannis Mitliagkas, and Leonidas J. Guibas. Learning representations and generative models for 3d point clouds. In *ICML*, volume 80 of *Proceedings of Machine Learning Research*, pages 40–49, Stockholm, Sweden, 2018. PMLR. 2



- [2] Noam Aigerman, Roi Poranne, and Yaron Lipman. Lifted bijections for low distortion surface mappings. *ACM Trans. Graph.*, 33(4), jul 2014. [2](#)
- [3] Thiemo Alldieck, Hongyi Xu, and Cristian Sminchisescu. imghum: Implicit generative models of 3d human shape and articulated pose. In *ICCV*, pages 5441–5450, Montreal, Canada, 2021. IEEE. [3](#)
- [4] Matan Atzmon and Yaron Lipman. Sal: Sign agnostic learning of shapes from raw data. In *IEEE/CVF Conference on Computer Vision and Pattern Recognition (CVPR)*, June 2020. [14](#)
- [5] Matan Atzmon and Yaron Lipman. SALD: sign agnostic learning with derivatives. In *9th International Conference on Learning Representations, ICLR 2021*, 2021. [5](#), [7](#), [14](#), [15](#), [16](#)
- [6] Matan Atzmon, David Novotný, Andrea Vedaldi, and Yaron Lipman. Augmenting implicit neural shape representations with explicit deformation fields, 2021. [3](#)
- [7] Chandrajit Bajaj, Tingran Gao, Zihang He, Qixing Huang, and Zhenxiao Liang. SMAC: simultaneous mapping and clustering using spectral decompositions. In *Proceedings of the 35th International Conference on Machine Learning, ICML 2018*, pages 334–343, Stockholm, Sweden, 2018. PMLR. [2](#)
- [8] Mirela Ben-Chen, Adrian Butscher, Justin Solomon, and Leonidas J. Guibas. On discrete killing vector fields and patterns on surfaces. *Comput. Graph. Forum*, 29(5):1701–1711, 2010. [3](#)
- [9] Federica Bogo, Javier Romero, Matthew Loper, and Michael J. Black. FAUST: Dataset and evaluation for 3D mesh registration. In *Proceedings IEEE Conf. on Computer Vision and Pattern Recognition (CVPR)*, Piscataway, NJ, USA, June 2014. IEEE. [7](#)
- [10] Ruojin Cai, Guandao Yang, Hadar Averbuch-Elor, Zekun Hao, Serge Belongie, Noah Snavely, and Bharath Hariharan. Learning gradient fields for shape generation. In *Computer Vision–ECCV 2020: 16th European Conference, Glasgow, UK, August 23–28, 2020, Proceedings, Part III 16*, pages 364–381. Springer, 2020. [7](#)
- [11] Yuxin Chen, Leonidas J. Guibas, and Qi-Xing Huang. Near-optimal joint object matching via convex relaxation. In *ICML*, volume 32 of *JMLR Workshop and Conference Proceedings*, pages 100–108, Beijing, China, 2014. JMLR.org. [2](#)
- [12] Zhiqin Chen and Hao Zhang. Learning implicit fields for generative shape modeling. In *IEEE Conference on Computer Vision and Pattern Recognition, CVPR 2019, Long Beach, CA, USA, June 16–20, 2019*, pages 5939–5948, Long Beach, CA, USA, 2019. Computer Vision Foundation / IEEE. [3](#)
- [13] An-Chieh Cheng, Xueting Li, Min Sun, Ming-Hsuan Yang, and Sifei Liu. Learning 3d dense correspondence via canonical point autoencoder, 2021. [3](#)
- [14] Christopher B. Choy, JunYoung Gwak, Silvio Savarese, and Manmohan Krishna Chandraker. Universal correspondence network. In *NIPS*, pages 2406–2414, Red Hook, NY, USA, 2016. Curran Associates Inc. [3](#)
- [15] Yu Deng, Jiaolong Yang, and Xin Tong. Deformed implicit field: Modeling 3d shapes with learned dense correspondence. In *CVPR*, pages 10286–10296, Virtual, 2021. Computer Vision Foundation / IEEE. [3](#)
- [16] Nicolas Donati, Abhishek Sharma, and Maks Ovsjanikov. Deep geometric functional maps: Robust feature learning for shape correspondence. In *CVPR*, pages 8589–8598, Washington, DC, NY, 2020. Computer Vision Foundation / IEEE. [2](#)
- [17] Nicolas Donati, Abhishek Sharma, and Maks Ovsjanikov. Deep geometric functional maps: Robust feature learning for shape correspondence. In *IEEE/CVF Conference on Computer Vision and Pattern Recognition (CVPR)*, June 2020. [7](#)
- [18] Marvin Eisenberger and Daniel Cremers. Hamiltonian dynamics for real-world shape interpolation. In Andrea Vedaldi, Horst Bischof, Thomas Brox, and Jan-Michael Frahm, editors, *Computer Vision - ECCV 2020 - 16th European Conference, Glasgow, UK, August 23–28, 2020, Proceedings, Part IV*, volume 12349 of *Lecture Notes in Computer Science*, pages 179–196, Virtual, 2020. Springer. [2](#)
- [19] Marvin Eisenberger, Zorah Löhner, and Daniel Cremers. Divergence-free shape correspondence by deformation. *Comput. Graph. Forum*, 38(5):1–12, 2019. [2](#)
- [20] Marvin Eisenberger, Zorah Lahner, and Daniel Cremers. Smooth shells: Multi-scale shape registration with functional maps. In *IEEE/CVF Conference on Computer Vision and Pattern Recognition (CVPR)*, June 2020. [7](#)
- [21] Marvin Eisenberger, David Novotný, Gael Kerchenbaum, Patrick Labatut, Natalia Neverova, Daniel Cremers, and Andrea Vedaldi. Neuromorph: Unsupervised shape interpolation and correspondence in one go. In *CVPR*, pages 7473–7483, Washington, DC, USA, 2021. Computer Vision Foundation / IEEE. [1](#), [2](#), [6](#), [7](#)
- [22] Marvin Eisenberger, David Novotny, Gael Kerchenbaum, Patrick Labatut, Natalia Neverova, Daniel Cremers, and Andrea Vedaldi. Neuromorph: Unsupervised shape interpolation and correspondence in one go. In *Proceedings of the IEEE/CVF Conference on Computer Vision and Pattern Recognition (CVPR)*, pages 7473–7483, Virtual, June 2021. Computer Vision Foundation / IEEE. [8](#), [14](#), [16](#)
- [23] Marvin Eisenberger, Aysim Toker, Laura Leal-Taixé, and Daniel Cremers. Deep shells: Unsupervised shape correspondence with optimal transport. In Hugo Larochelle, Marc’Aurelio Ranzato, Raia Hadsell, Maria-Florina Balcan, and Hsuan-Tien Lin, editors, *Advances in Neural Information Processing Systems 33: Annual Conference on Neural Information Processing Systems 2020, NeurIPS 2020, December 6–12, 2020*, pages 10491–10502, Virtual, 2020. Curran Associates, Inc. [7](#)
- [24] Haoqiang Fan, Hao Su, and Leonidas J. Guibas. A point set generation network for 3d object reconstruction from a single image. In *CVPR*, pages 2463–2471, Honolulu, Hawaii, 2017. IEEE Computer Society. [2](#)
- [25] Maolin Gao, Zorah Lahner, Johan Thunberg, Daniel Cremers, and Florian Bernard. Isometric multi-shape matching. In *Proceedings of the IEEE/CVF Conference on Computer Vision and Pattern Recognition (CVPR)*, pages 14183–14193, Virtual, June 2021. Computer Vision Foundation / IEEE. [6](#), [7](#)
- [26] Michael Garland and Paul S. Heckbert. Surface simplification using quadric error metrics. In *Proceedings of the 24th Annual Conference on Computer Graphics and Interactive Techniques, SIGGRAPH 1997, Los Angeles, CA, USA, August 3–8, 1997*, pages 209–216. ACM, 1997. [13](#)
- [27] Amos Gropp, Lior Yariv, Niv Haim, Matan Atzmon, and Yaron Lipman. Implicit geometric regularization for learning shapes. In *ICML*, volume 119 of *Proceedings of Machine Learning Research*, pages 3789–3799, Virtual, 2020. PMLR. [3](#)

- [28] Amos Gropp, Lior Yariv, Niv Haim, Matan Atzmon, and Yaron Lipman. Implicit geometric regularization for learning shapes. In *Proceedings of Machine Learning and Systems 2020*, pages 3569–3579. 2020. [14](#)
- [29] Thibault Groueix, Matthew Fisher, Vladimir G. Kim, Bryan C. Russell, and Mathieu Aubry. 3d-coded: 3d correspondences by deep deformation. In *ECCV (2)*, volume 11206 of *Lecture Notes in Computer Science*, pages 235–251, Virtual, 2018. Springer. [3](#)
- [30] Thibault Groueix, Matthew Fisher, Vladimir G. Kim, Bryan C. Russell, and Mathieu Aubry. 3d-coded: 3d correspondences by deep deformation. In *Proceedings of the European Conference on Computer Vision (ECCV)*, September 2018. [7](#)
- [31] Thibault Groueix, Matthew Fisher, Vladimir G. Kim, Bryan C. Russell, and Mathieu Aubry. 3d-coded: 3d correspondences by deep deformation. In *ECCV (2)*, volume 11206 of *Lecture Notes in Computer Science*, pages 235–251, New York, NY, USA, 2018. Springer. [7](#)
- [32] Oshri Halimi, Or Litany, Emanuele Rodolà, Alexander M. Bronstein, and Ron Kimmel. Unsupervised learning of dense shape correspondence. In *CVPR*, pages 4370–4379, Long Beach, CA, 2019. Computer Vision Foundation / IEEE. [2](#)
- [33] Oshri Halimi, Or Litany, Emanuele Rodola, Alex M. Bronstein, and Ron Kimmel. Unsupervised learning of dense shape correspondence. In *Proceedings of the IEEE/CVF Conference on Computer Vision and Pattern Recognition (CVPR)*, June 2019. [7](#)
- [34] Qixing Huang, Bart Adams, Martin Wicke, and Leonidas J. Guibas. Non-rigid registration under isometric deformations. *Comput. Graph. Forum*, 27(5):1449–1457, 2008. [13](#)
- [35] Qi-Xing Huang and Leonidas J. Guibas. Consistent shape maps via semidefinite programming. *Comput. Graph. Forum*, 32(5):177–186, 2013. [1](#), [2](#), [5](#)
- [36] Qixing Huang, Xiangru Huang, Bo Sun, Zaiwei Zhang, Junfeng Jiang, and Chandrajit Bajaj. Arapreg: An as-rigid-as possible regularization loss for learning deformable shape generators. In *Proceedings of the IEEE/CVF International Conference on Computer Vision (ICCV)*, pages 5815–5825, Virtual, October 2021. Computer Vision Foundation / IEEE. [3](#), [4](#), [5](#), [6](#), [13](#), [14](#)
- [37] Qixing Huang, Xiangru Huang, Bo Sun, Zaiwei Zhang, Junfeng Jiang, and Chandrajit Bajaj. Arapreg: An as-rigid-as possible regularization loss for learning deformable shape generators. In *Proceedings of the IEEE/CVF international conference on computer vision*, pages 5815–5825, 2021. [4](#)
- [38] Qixing Huang, Zhenxiao Liang, Haoyun Wang, Simiao Zuo, and Chandrajit Bajaj. Tensor maps for synchronizing heterogeneous shape collections. *ACM Trans. Graph.*, 38(4), jul 2019. [1](#)
- [39] Qixing Huang, Fan Wang, and Leonidas J. Guibas. Functional map networks for analyzing and exploring large shape collections. *ACM Trans. Graph.*, 33(4):36:1–36:11, 2014. [1](#), [2](#)
- [40] Qi-Xing Huang, Martin Wicke, Bart Adams, and Leonidas Guibas. Shape Decomposition using Modal Analysis. *Computer Graphics Forum*, 28(2):407–416, 2009. [4](#)
- [41] Qi-Xing Huang, Guo-Xin Zhang, Lin Gao, Shi-Min Hu, Adrian Butscher, and Leonidas Guibas. An optimization approach for extracting and encoding consistent maps in a shape collection. *ACM Trans. Graph.*, 31(6), nov 2012. [1](#), [2](#)
- [42] Ruqi Huang, Jing Ren, Peter Wonka, and Maks Ovsjanikov. Consistent zoomout: Efficient spectral map synchronization. *Comput. Graph. Forum*, 39(5):265–278, 2020. [1](#), [2](#)
- [43] Ruqi Huang, Jing Ren, Peter Wonka, and Maks Ovsjanikov. Consistent zoomout: Efficient spectral map synchronization. *Comput. Graph. Forum*, 39(5):265–278, 2020. [6](#), [7](#)
- [44] Xiangru Huang, Zhenxiao Liang, Chandrajit Bajaj, and Qixing Huang. Translation synchronization via truncated least squares. In I. Guyon, U. V. Luxburg, S. Bengio, H. Wallach, R. Fergus, S. Vishwanathan, and R. Garnett, editors, *Advances in Neural Information Processing Systems 30*, pages 1459–1468. Curran Associates Inc., Red Hook, NY, USA, 2017. [2](#)
- [45] Xiangru Huang, Zhenxiao Liang, and Qixing Huang. Uncertainty quantification for multi-scan registration. *ACM Trans. Graph.*, 39(4), July 2020. [1](#), [2](#)
- [46] Xiangru Huang, Zhenxiao Liang, Xiaowei Zhou, Yao Xie, Leonidas J. Guibas, and Qixing Huang. Learning transformation synchronization. In *The IEEE Conference on Computer Vision and Pattern Recognition (CVPR)*, pages 8082–8091, Virtual, 2019. Computer Vision Foundation / IEEE. [1](#), [2](#)
- [47] Vladimir G. Kim, Wilmot Li, Niloy J. Mitra, Stephen DiVerdi, and Thomas Funkhouser. Exploring collections of 3d models using fuzzy correspondences. *ACM Trans. Graph.*, 31(4), jul 2012. [1](#), [2](#)
- [48] Vladimir G. Kim, Yaron Lipman, and Thomas Funkhouser. Blended intrinsic maps. *ACM Trans. Graph.*, 30(4), jul 2011. [2](#)
- [49] Vladislav Kraevoy and Alla Sheffer. Cross-parameterization and compatible remeshing of 3d models. *ACM Trans. Graph.*, 23(3):861–869, aug 2004. [1](#)
- [50] Chun-Liang Li, Manzil Zaheer, Yang Zhang, Barnabás Póczos, and Ruslan Salakhutdinov. Point cloud GAN, 2019. [2](#)
- [51] Lei Li, Nicolas Donati, and Maks Ovsjanikov. Learning multi-resolution functional maps with spectral attention for robust shape matching. In *Advances in Neural Information Processing Systems 35: Annual Conference on Neural Information Processing Systems 2022, NeurIPS 2022, 8-14 December 2022, Vancouver, BC, Canada*, pages 1–10, Red Hook, NY, USA, 2022. Curran Associates Inc. [7](#)
- [52] Ruihui Li, Xianzhi Li, Chi-Wing Fu, Daniel Cohen-Or, and Pheng-Ann Heng. PU-GAN: A point cloud upsampling adversarial network. In *ICCV*, pages 7202–7211, Seoul, Republic of Korea, 2019. IEEE. [2](#)
- [53] Or Litany, Alexander M. Bronstein, Michael M. Bronstein, and Ameesh Makadia. Deformable shape completion with graph convolutional autoencoders. In *2018 IEEE Conference on Computer Vision and Pattern Recognition, CVPR 2018, Salt Lake City, UT, USA, June 18-22, 2018*, pages 1886–1895, Salt Lake City, UT, USA, 2018. IEEE Computer Society. [2](#)
- [54] Or Litany, Tal Remez, Emanuele Rodola, Alex Bronstein, and Michael Bronstein. Deep functional maps: Structured prediction for dense shape correspondence. In *Proceedings of the IEEE International Conference on Computer Vision (ICCV)*, Oct 2017. [7](#)
- [55] Or Litany, Tal Remez, Emanuele Rodolà, Alexander M. Bronstein, and Michael M. Bronstein. Deep functional maps: Structured prediction for dense shape correspondence. In *ICCV*, pages 5660–5668, Washington, DC, USA, 2017. IEEE Computer Society. [2](#)
- [56] Feng Liu and Xiaoming Liu. Learning implicit functions for topology-varying dense 3d shape correspondence. In

- NeurIPS*, pages 4823–4834, Red Hook, NY, USA, 2020. Curran Associates Inc. **3**
- [57] William E. Lorensen and Harvey E. Cline. Marching cubes: A high resolution 3d surface construction algorithm. In Maureen C. Stone, editor, *Proceedings of the 14th Annual Conference on Computer Graphics and Interactive Techniques, SIGGRAPH 1987, Anaheim, California, USA, July 27-31, 1987*, pages 163–169, New York, NY, 1987. ACM. **4**
- [58] Shitong Luo and Wei Hu. Diffusion probabilistic models for 3d point cloud generation. In *Proceedings of the IEEE/CVF Conference on Computer Vision and Pattern Recognition*, pages 2837–2845, 2021. **7**
- [59] Haggai Maron, Nadav Dym, Itay Kezurer, Shahar Z. Kovalsky, and Yaron Lipman. Point registration via efficient convex relaxation. *ACM Trans. Graph.*, 35(4):73:1–73:12, 2016. **2**
- [60] Simone Melzi, Jing Ren, Emanuele Rodolà, Abhishek Sharma, Peter Wonka, and Maks Ovsjanikov. Zoomout: spectral upsampling for efficient shape correspondence. *ACM Trans. Graph.*, 38(6):155:1–155:14, 2019. **2, 7**
- [61] Lars M. Mescheder, Michael Oechsle, Michael Niemeyer, Sebastian Nowozin, and Andreas Geiger. Occupancy networks: Learning 3d reconstruction in function space. In *CVPR*, pages 4460–4470, Long Beach, California, 2019. Computer Vision Foundation / IEEE. **3**
- [62] Andy Nguyen, Mirela Ben-Chen, Katarzyna Welnicka, Yinyu Ye, and Leonidas J. Guibas. An optimization approach to improving collections of shape maps. *Comput. Graph. Forum*, 30(5):1481–1491, 2011. **1, 2**
- [63] Maks Ovsjanikov, Mirela Ben-Chen, Justin Solomon, Adrian Butscher, and Leonidas Guibas. Functional maps: A flexible representation of maps between shapes. *ACM Trans. Graph.*, 31(4), jul 2012. **2, 7**
- [64] Deepti Pachauri, Risi Kondor, and Vikas Singh. Solving the multi-way matching problem by permutation synchronization. In *NIPS*, pages 1860–1868, Red Hook, NY, USA, 2013. Curran Associates Inc. **2**
- [65] Jeong Joon Park, Peter Florence, Julian Straub, Richard A. Newcombe, and Steven Lovegrove. Deepsdf: Learning continuous signed distance functions for shape representation. In *IEEE Conference on Computer Vision and Pattern Recognition, CVPR 2019, Long Beach, CA, USA, June 16-20, 2019*, pages 165–174, Long Beach, California, 2019. Computer Vision Foundation / IEEE. **3, 7**
- [66] Adam Paszke, Sam Gross, Francisco Massa, Adam Lerer, James Bradbury, Gregory Chanan, Trevor Killeen, Zeming Lin, Natalia Gimelshein, Luca Antiga, Alban Desmaison, Andreas Köpf, Edward Z. Yang, Zachary DeVito, Martin Raison, Alykhan Tejani, Sasank Chilamkurthy, Benoit Steiner, Lu Fang, Junjie Bai, and Soumith Chintala. Pytorch: An imperative style, high-performance deep learning library. In *Annual Conference on Neural Information Processing Systems 2019, NeurIPS 2019, December 8-14, 2019, Vancouver, BC, Canada*, pages 8024–8035, 2019. **5, 13**
- [67] Sida Peng, Yuanqing Zhang, Yinghao Xu, Qianqian Wang, Qing Shuai, Hujun Bao, and Xiaowei Zhou. Neural body: Implicit neural representations with structured latent codes for novel view synthesis of dynamic humans. In *CVPR*, pages 9054–9063, Washington, DC, 2021. Computer Vision Foundation / IEEE. **3**
- [68] Charles R. Qi, Hao Su, Kaichun Mo, and Leonidas J. Guibas. Pointnet: Deep learning on point sets for 3d classification and segmentation. In *Proceedings of the IEEE Conference on Computer Vision and Pattern Recognition (CVPR)*, July 2017. **5**
- [69] Marie-Julie Rakotosaona and Maks Ovsjanikov. Intrinsic point cloud interpolation via dual latent space navigation. In Andrea Vedaldi, Horst Bischof, Thomas Brox, and Jan-Michael Frahm, editors, *Computer Vision - ECCV 2020 - 16th European Conference, Glasgow, UK, August 23-28, 2020, Proceedings, Part II*, volume 12347 of *Lecture Notes in Computer Science*, pages 655–672, New York, NY, 2020. Springer. **2**
- [70] Anurag Ranjan, Timo Bolkart, Soubhik Sanyal, and Michael J. Black. Generating 3d faces using convolutional mesh autoencoders. In Vittorio Ferrari, Martial Hebert, Cristian Sminchisescu, and Yair Weiss, editors, *Computer Vision - ECCV 2018 - 15th European Conference, Munich, Germany, September 8-14, 2018, Proceedings, Part III*, volume 11207 of *Lecture Notes in Computer Science*, pages 725–741, New York, NY, 2018. Springer. **14**
- [71] Jing Ren, Adrien Poulenard, Peter Wonka, and Maks Ovsjanikov. Continuous and orientation-preserving correspondences via functional maps. *ACM Trans. Graph.*, 37(6), dec 2018. **6, 7**
- [72] Jean-Michel Roufousse, Abhishek Sharma, and Maks Ovsjanikov. Unsupervised deep learning for structured shape matching. In *Proceedings of the IEEE/CVF International Conference on Computer Vision (ICCV)*, October 2019. **7**
- [73] Yusuf Sahillioglu. Recent advances in shape correspondence. *Vis. Comput.*, 36(8):1705–1721, 2020. **2**
- [74] Shunsuke Saito, Zeng Huang, Ryota Natsume, Shigeo Morishima, Hao Li, and Angjoo Kanazawa. Pifu: Pixel-aligned implicit function for high-resolution clothed human digitization. In *ICCV*, pages 2304–2314, Seoul, Republic of Korea, 2019. IEEE. **3**
- [75] Shunsuke Saito, Tomas Simon, Jason M. Saragih, and Hanbyul Joo. Pifuhd: Multi-level pixel-aligned implicit function for high-resolution 3d human digitization. In *CVPR*, pages 81–90, Washington, DC, 2020. Computer Vision Foundation / IEEE. **3**
- [76] John Schreiner, Arul Asirvatham, Emil Praun, and Hugues Hoppe. Inter-surface mapping. In *ACM SIGGRAPH 2004 Papers, SIGGRAPH '04*, page 870–877, New York, NY, USA, 2004. Association for Computing Machinery. **1**
- [77] Abhishek Sharma and Maks Ovsjanikov. Weakly supervised deep functional maps for shape matching. In Hugo Larochelle, Marc’Aurelio Ranzato, Raia Hadsell, Maria-Florina Balcan, and Hsuan-Tien Lin, editors, *Advances in Neural Information Processing Systems 33: Annual Conference on Neural Information Processing Systems 2020, NeurIPS 2020, December 6-12, 2020, virtual*, pages 19264–19275, Red Hook, NY, USA, 2020. Curran Associates Inc. **2**
- [78] Miroslava Slavcheva, Maximilian Baust, Daniel Cremers, and Slobodan Ilic. Killingfusion: Non-rigid 3d reconstruction without correspondences. In *2017 IEEE Conference on Computer Vision and Pattern Recognition, CVPR 2017, Honolulu, HI, USA, July 21-26, 2017*, pages 5474–5483, Washington, DC, 2017. IEEE Computer Society. **3**
- [79] Justin Solomon, Mirela Ben-Chen, Adrian Butscher, and Leonidas J. Guibas. As-killing-as-possible vector fields for planar deformation. *Comput. Graph. Forum*, 30(5):1543–1552, 2011. **3**
- [80] Olga Sorkine and Marc Alexa. As-rigid-as-possible surface modeling. In *Proceedings of the Fifth Eurographics Sympo-*



- sium on Geometry Processing, Barcelona, Spain, July 4-6, 2007*, volume 257, pages 109–116, 2007. 13
- [81] Jos Stam and Ryan M. Schmidt. On the velocity of an implicit surface. *ACM Trans. Graph.*, 30(3):21:1–21:7, 2011. 3, 4
- [82] Robert W Sumner and Jovan Popović. Deformation transfer for triangle meshes. *ACM Transactions on graphics (TOG)*, 23(3):399–405, 2004. 1
- [83] Qingyang Tan, Lin Gao, Yu-Kun Lai, and Shihong Xia. Variational autoencoders for deforming 3d mesh models. In *2018 IEEE Conference on Computer Vision and Pattern Recognition, CVPR 2018, Salt Lake City, UT, USA, June 18-22, 2018*, pages 5841–5850, Salt Lake City, UT, USA, 2018. IEEE Computer Society. 2
- [84] Michael Tao, Justin Solomon, and Adrian Butscher. Near-isometric level set tracking. *Comput. Graph. Forum*, 35(5):65–77, 2016. 3, 4
- [85] Edgar Tretschk, Ayush Tewari, Michael Zollhöfer, Vladislav Golyanik, and Christian Theobalt. DEMA: deep mesh autoencoders for non-rigidly deforming objects. In Andrea Vedaldi, Horst Bischof, Thomas Brox, and Jan-Michael Frahm, editors, *Computer Vision - ECCV 2020 - 16th European Conference, Glasgow, UK, August 23-28, 2020, Proceedings, Part IV*, volume 12349 of *Lecture Notes in Computer Science*, pages 601–617, Glasgow, UK, 2020. Springer. 2
- [86] Oliver van Kaick, Hao Zhang, Ghassan Hamarneh, and Daniel Cohen-Or. A survey on shape correspondence. In Helwig Hauser and Erik Reinhard, editors, *31st Annual Conference of the European Association for Computer Graphics, Eurographics 2010 - State of the Art Reports, Norrköping, Sweden, May 3-7, 2010*, pages 61–82, 9105 Salley Street Montreal, Quebec H8R 2C8 CANADA, 2010. Eurographics Association. 2
- [87] Nitika Verma, Edmond Boyer, and Jakob Verbeek. Featnet: Feature-steered graph convolutions for 3d shape analysis. In *2018 IEEE Conference on Computer Vision and Pattern Recognition, CVPR 2018, Salt Lake City, UT, USA, June 18-22, 2018*, pages 2598–2606, Salt Lake City, UT, USA, 2018. IEEE Computer Society. 2
- [88] Matthias Vestner, Roei Litman, Emanuele Rodola, Alex Bronstein, and Daniel Cremers. Product manifold filter: Non-rigid shape correspondence via kernel density estimation in the product space. In *Proceedings of the IEEE Conference on Computer Vision and Pattern Recognition (CVPR)*, July 2017. 7
- [89] Lanhui Wang and Amit Singer. Exact and stable recovery of rotations for robust synchronization. *Information and Inference: A Journal of the IMA*, 2:145–193, December 2013. 1, 2
- [90] Lingyu Wei, Qixing Huang, Duygu Ceylan, Etienne Vouga, and Hao Li. Dense human body correspondences using convolutional networks. In *CVPR*, pages 1544–1553, Washington, DC, 2016. IEEE Computer Society. 3
- [91] Yaoqing Yang, Chen Feng, Yiru Shen, and Dong Tian. Foldingnet: Point cloud auto-encoder via deep grid deformation. In *CVPR*, pages 206–215, Washington, DC, 2018. Computer Vision Foundation / IEEE Computer Society. 2
- [92] Yusuke Yoshidasu, Wan-Chun Ma, Eiichi Yoshida, and Fumio Kanehiro. As-conformal-as-possible surface registration. In *Proceedings of the Symposium on Geometry Processing, SGP '14*, page 257–267, Goslar, DEU, 2014. Eurographics Association. 4
- [93] Yi Zhou, Chenglei Wu, Zimo Li, Chen Cao, Yuting Ye, Jason M. Saragih, Hao Li, and Yaser Sheikh. Fully convolutional mesh autoencoder using efficient spatially varying kernels. In Hugo Larochelle, Marc’Aurelio Ranzato, Raia Hadsell, Maria-Florina Balcan, and Hsuan-Tien Lin, editors, *Advances in Neural Information Processing Systems 33: Annual Conference on Neural Information Processing Systems 2020, NeurIPS 2020, December 6-12, 2020, virtual*, pages 9251–9262, Red Hook, NY, USA, 2020. Curran Associates Inc. 14
- [94] Silvia Zuffi, Angjoo Kanazawa, David W. Jacobs, and Michael J. Black. 3d menagerie: Modeling the 3d shape and pose of animals. In *CVPR*, pages 5524–5532, Washington, DC, USA, 2017. IEEE Computer Society. 6



The supplementary materials provide more details of implementing the regularization loss used in the implicit shape generator in Section A and details of mesh generator initialization in Section B. Section C gives more details on the dataset preprocessing. Section D and Section E show more results on shape space learning and shape matching, respectively.

## A. Details of Regularization Loss

### A.1. Expression of $\bar{L}^{\text{arap}}(g^\phi(z))$

$$\bar{L}^{\text{arap}}(g^\phi(z)) = 2L \otimes I_3 - B^{\text{arap}}(g^\phi(z)) D^{\text{arap}}(g^\phi(z)) B^{\text{arap}}(g^\phi(z))^T,$$

where  $L$  is the graph Laplacian of the mesh, and  $B^{\text{arap}}(g^\phi(z)) \in \mathbb{R}^{3n \times 3n}$  is a sparse block matrix defined as

$$B_{ij}^{\text{arap}}(g^\phi(z)) = \begin{cases} \sum_{k \in \mathcal{N}_i} e_{ik}^\phi(z) \times & i = j \\ e_{ij}^\phi(z) \times & j \in \mathcal{N}_i \\ 0 & \text{else} \end{cases}$$

where  $e_{ij}^\phi(z) = g_i^\phi(z) - g_j^\phi(z)$  and  $D^{\text{arap}}(g^\phi(z)) \in \mathbb{R}^{3n \times 3n}$  is a diagonal block matrix defined as

$$D_{ii}^{\text{arap}}(g^\phi(z)) = \left( \sum_{j \in \mathcal{N}_i} (\|e_{ij}^\phi(z)\|^2 I_3 - e_{ij}^\phi(z) e_{ij}^\phi(z)^T) \right)^{-1}$$

### A.2. Expression of $\bar{L}^{\text{acap}}(g^\phi(z))$

$$\bar{L}^{\text{acap}}(g^\phi(z)) = 2L \otimes I_3 - B^{\text{acap}}(g^\phi(z)) D^{\text{acap}}(g^\phi(z)) B^{\text{acap}}(g^\phi(z))^T,$$

where  $B^{\text{acap}}(g^\phi(z)) \in \mathbb{R}^{3n \times 4n}$  is a sparse block matrix defined as

$$B_{ij}^{\text{acap}}(g^\phi(z)) = \begin{cases} \sum_{k \in \mathcal{N}_i} \begin{pmatrix} -e_{ik}^\phi(z) & e_{ik}^\phi(z) \times \end{pmatrix} & i = j \\ \begin{pmatrix} -e_{ij}^\phi(z) & e_{ij}^\phi(z) \times \end{pmatrix} & j \in \mathcal{N}_i \\ 0 & \text{else} \end{cases}$$

and  $D^{\text{acap}}(g^\phi(z)) \in \mathbb{R}^{4n \times 4n}$  is a diagonal block matrix defined as

$$D_{ii}^{\text{acap}}(g^\phi(z)) = \left( \sum_{j \in \mathcal{N}_i} (\|e_{ij}^\phi(z)\|^2 I_4 - \text{diag}(0, e_{ij}^\phi(z) e_{ij}^\phi(z)^T)) \right)^{-1}$$

## A.3. Implementation Details

Both the geometric deformation regularization  $r_{\text{geo}}(g^\phi)$  and the cycle-consistency regularization  $l_{\text{cyc}}(g^\phi)$  rely on the mesh with  $n$  vertices that is discretized from  $g^\phi(x, z) = 0$ . We use Marching Cube for discretization. For the human category, we use a voxel grid with size  $64 \times 77 \times 64$ . For the animal category, the size of the voxel grid is  $82 \times 50 \times 71$ . The output mesh of the Marching Cube algorithm typically contains more than 5000 vertices. To reduce the computation complexity, we simplify the output mesh into 2000 faces [26] before computing  $r_{\text{geo}}(g^\phi)$  and  $l_{\text{cyc}}(g^\phi)$ . The number of vertices  $n$  is around 1000, thus the size of  $\bar{L}^\phi(z)$  is around  $3000 \times 3000$ . Computing  $(\bar{L}^\phi(z))^+$  only takes about 40ms in PyTorch [66]

## B. Details of Mesh Generator Initialization

### B.1. Template-based Registration

In order to register the template mesh  $\mathcal{M}$  to the input shape  $S_i$ , we first generate  $m$  intermediate shape  $g^\phi(z_i^j)$ , where  $z_i^j = z_{\text{temp}} + j \frac{z_i - z_{\text{temp}}}{m+1}$ ,  $1 \leq j \leq m$ . Instead of directly register  $\mathcal{M}$  to  $S_i$ , we first register  $\mathcal{M}$  to  $g^\phi(z_i^1)$  with ACAP deformation energy [80, 34]. Since  $\mathcal{M}$  and  $g^\phi(z_i^1)$  are very close, we directly apply nearest neighbor search to compute the correspondence for the data term. The registration gives the resulting deformed template  $\mathcal{M}_1$ . We then register  $\mathcal{M}_1$  to  $g^\phi(z_i^2)$  and get the deformed template  $\mathcal{M}_2$ , register  $\mathcal{M}_2$  to  $g^\phi(z_i^3)$  and get the deformed template  $\mathcal{M}_3$ , and so on and so forth. Finally we get the deformed template  $\mathcal{M}_m$ , which is well-aligned with  $S_i$ .

The interpolation-guided registration typically works well but might fail when the template  $\mathcal{M}$  is too far from  $S_i$ , i.e. the two shapes have very different poses. The reason is that the intermediate shapes on the interpolation path might not have good quality. To make full use of the learned shape space, we add shapes from the input shape collection to the interpolation path in these cases. First, we compute the distance between each pair of shape  $S_i$  and  $S_j$  using the distance of their embedded latent codes  $\|z_i - z_j\|$ . Based on this distance metric, we build a  $K$ -NN graph among the input shape collection. We set  $K = 25$  for the human dataset and  $K = 40$  for the animal dataset. We then perform interpolation-guided registration on each edge  $(i, j)$  of the graph and obtain the correspondences between  $S_i$  and  $S_j$ . We use the distortion of the mapped edges [34] as the weights in the  $K$ -NN graph. Finally we compute the shortest path from the template to each shape  $S_i$  and get the correspondence by composing the correspondences along the shortest path.

### B.2. Mesh Generator Architecture

The network architecture of  $g^\theta$  follows from that in [36], which outputs displacements of vertex positions of the template mesh  $\mathcal{M}$ . We sample 4 resolutions of the mesh connections of the template mesh. The network architecture stacks 4 blocks of convolution + up-sampling layers. The

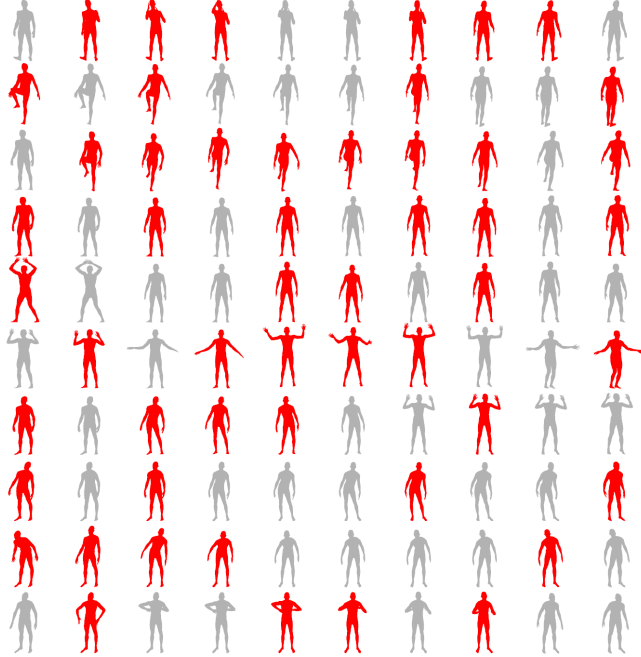


Figure 6. We use FPS to further select a more diverse and challenging subset of 1000 shapes from the training split [5, 4, 28]. In this example, among  $10 \times 10 = 100$  shapes from the training split [5, 4, 28], only the red shapes are selected because the gray shapes have similar poses.

convolution layer employs Chebyshev convolutional filters with  $K = 6$  Chebyshev polynomials [70]. Similar to [93], there is a fully connected layer between the latent code and the input to the first convolution layer.

### C. Details of Datasets

There are approximately 41k shapes in the original DFAUST dataset. Since there is low variety between the adjacent shapes, recent works [5, 4, 28] create a new training/testing split by uniformly sample 20% shapes from the original dataset. However, we notice that there are still many similar shapes in the splits. For example, almost all motion sequences start from shapes with very similar rest pose. In order to make the dataset more challenging, we further select 1000 shapes from the training split. Specifically, we first learn a VAE [5] to embed all the shapes from the training split into different latent vectors. We find that the latent vectors of similar shapes are typically closer. Then we apply farthest point sampling (FPS) to the latent vectors and select the first 1000 shapes. An example is shown in Figure 6. We apply the same approach to the testing split and select another 1000 shapes for testing.

The original SMAL dataset from [36] contains 300 training shapes and 100 testing shapes. We filter out the shapes that have unreasonable self-intersection, leading to 289 training shapes and 94 testing shapes.

For both DFAUST and SMAL dataset, we evaluate the correspondences from a template shape to the remaining shapes.

### D. More Results of Shape Space Learning

We show the shape interpolation results of SOTA implicit generator [5] and our method in Figure 7 and Figure 8. We show 30 interpolated shapes. By adding the proposed geometric deformation regularization loss and cycle-consistency regularization loss, our generator gives more meaningful interpolation results, which are important to the interpolation-guided registration.

### E. More Results of Shape Matching

We show the correspondence results of NeuroMorph [22] and our method in Figure 9 and Figure 10. Our method has lower errors compared to NeuroMorph.

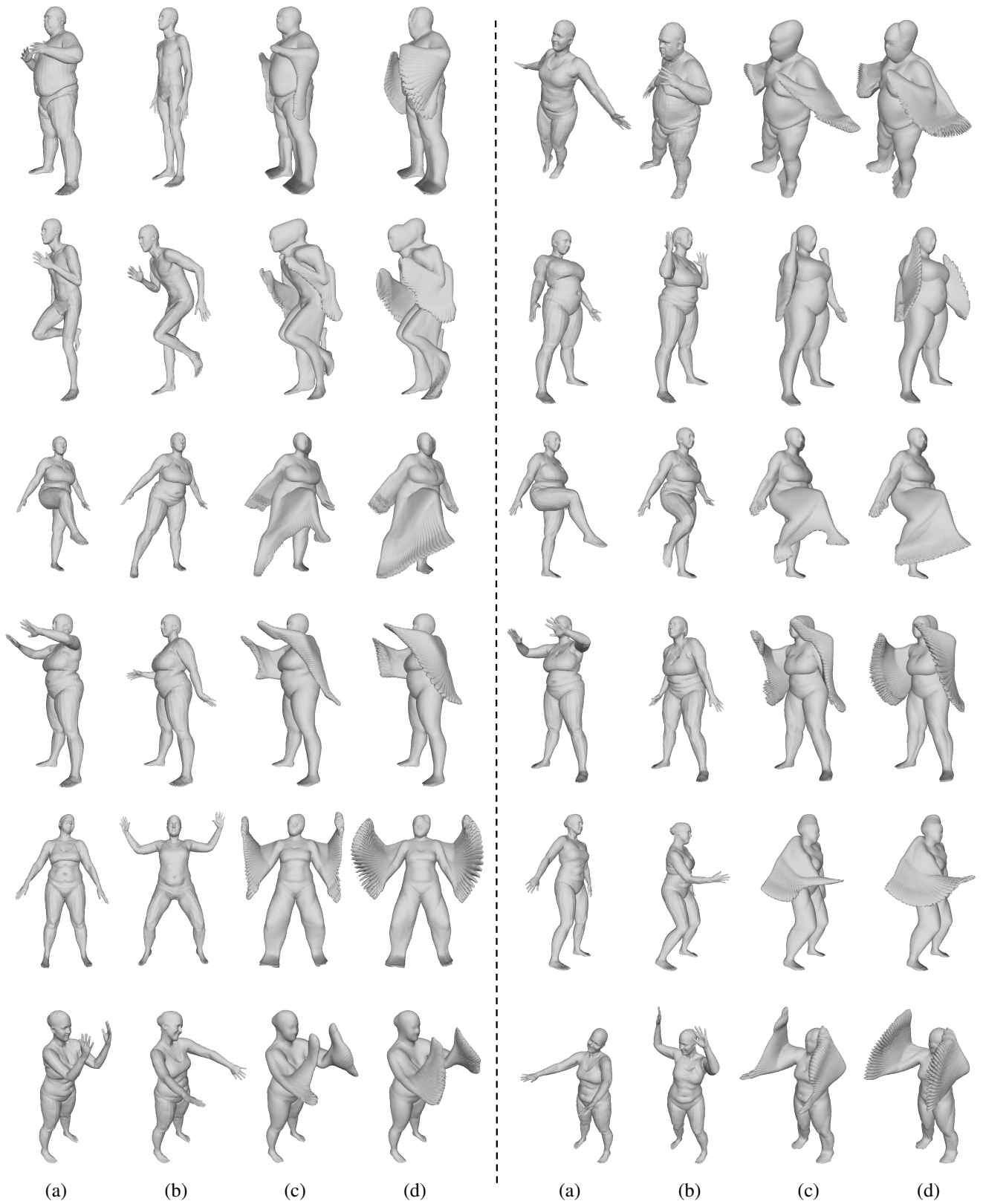


Figure 7. The comparison of shape interpolation between SALD [5] and our method on the DFAUST dataset. (a) source shape. (b) target shape. (c) interpolation results of SALD [5]. (d) our results.

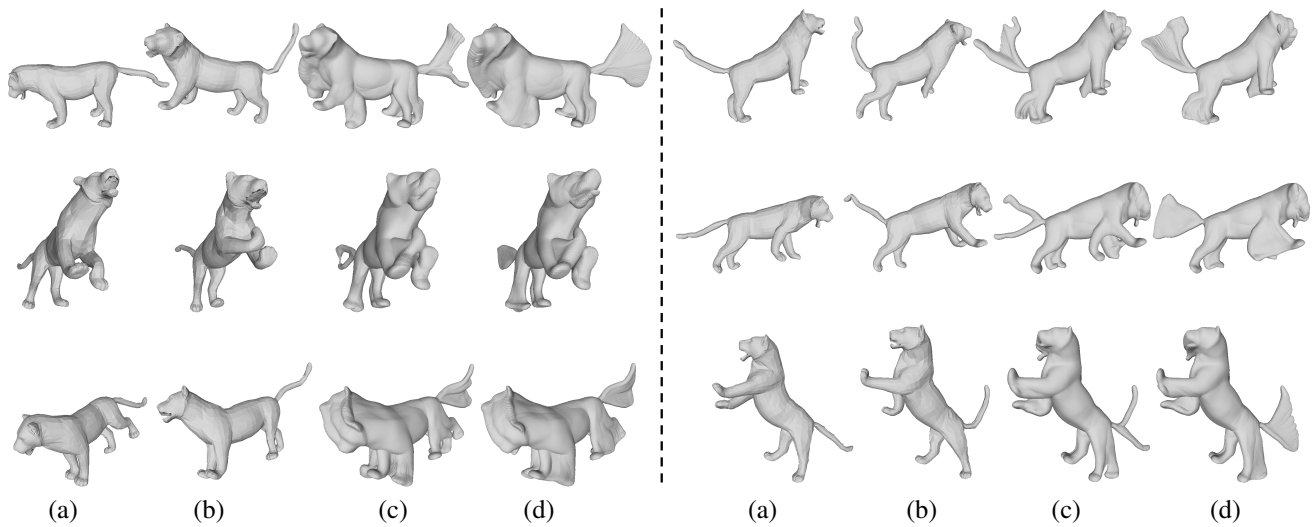


Figure 8. The comparison of shape interpolation between SALD [5] and our method on the SMAL dataset. (a) source shape. (b) target shape. (c) interpolation results of SALD [5]. (d) our results.

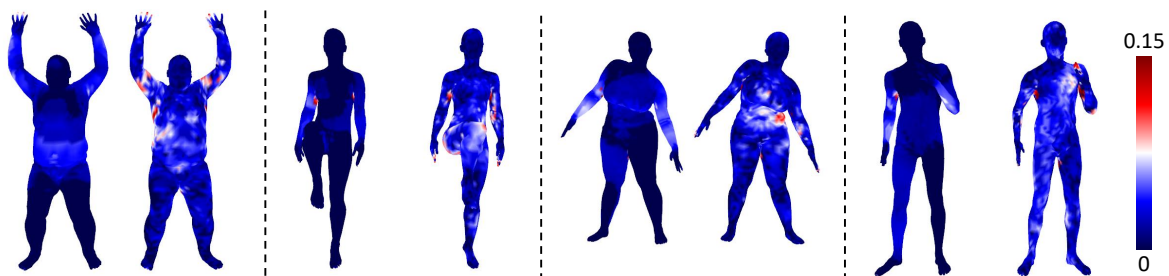


Figure 9. The comparison of the correspondences between our method and NeuroMorph [22] on the DFAUST dataset. We show the correspondence errors on the target shapes. For each group of shapes, the left is our result, the right is from NeuroMorph.

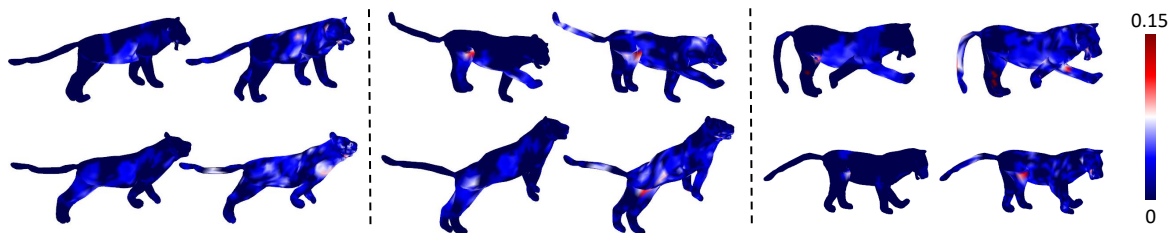


Figure 10. The comparison of the correspondences between our method and NeuroMorph [22] on the SMAL dataset. We show the correspondence errors on the target shapes. For each group of shapes, the left is our result, the right is from NeuroMorph.